Heliyon 9 (2023) e17678

Contents lists available at ScienceDirect

Heliyon

journal homepage: www.cell.com/heliyon

Numerical investigation of chemically reacting jet flow of hybrid nanofluid under the significances of bio-active mixers and chemical reaction

Nidhish Kumar Mishra [a], Sadia Anwar [b], Poom Kumam [c,d,**], Thidaporn Seangwattana [e,*], Muhammad Bilal [f], Anwar Saeed [c]

[a] Department of Basic Sciences, College of Science and Theoretical Studies, Saudi Electronic University, (Jeddah-M), Riyadh, 11673, Kingdom of Saudi Arabia

[b] Department of Mathematics, College of Arts and Sciences, Wadi Ad Dawasir (11991), Prince Sattam Bin Abdulaziz University, Al-Kharj, Kingdom of Saudi Arabia

[c] Center of Excellence in Theoretical and Computational Science (TaCS-CoE), Science Laboratory Building, King Mongkut's University of Technology Thonburi (KMUTT), 126 Pracha-Uthit Road, Bang Mod, Thung Khru, Bangkok, 10140, Thailand

[d] Department of Medical Research, China Medical University Hospital, China Medical University, Taichung, 40402, Taiwan

[e] Faculty of Science Energy and Environment, King Mongkut's University of Technology North Bangkok, Rayong Campus (KMUTNB), 21120, Rayong, Thailand

[f] Sheikh Taimur Academic Block-II, Department of Mathematics, University of Peshawar, Khyber Pakhtunkhwa, Pakistan

ARTICLE INFO

Keywords:
Modified Boungiorno model
bvp4c package
Activation energy
Jet flow
Hybrid nanofluid
Second order chemical reaction

ABSTRACT

Jet flows are employed in a variety of applications. It can be found in daily life as well as in agriculture, for example, jet flow assists with irrigation and harvest protection. The current problem is related to the study of energy and mass transference on the hybrid nanoliquid flow with mixed convection effect due to the vertical stretching surface conveying the cobalt ferrite $CoFe_2O_4$ and titanium dioxide TiO_2 nanoparticles (NPs) with the base fluid water H_2O. Further, the role of the chemical reaction, heat source/sink, and activation energy are investigated. By exploiting the idea of the modified Buongiorno model, the thermophoretic and Brownian diffusivity effects have discoursed on the existing flow behavior. The existing mathematical problem is framed with the application of the nonlinear higher-order PDEs. Higher-order PDEs of the mathematical model are changed into highly nonlinear ODEs by using the concepts of suitable similarity transformations. The modified higher-order nonlinear ODEs are cracked by manipulating the bvp4c technique in MATLAB. The impacts of the numerous physical flow parameters on the velocity, energy, and concentration are computed in graphical forms. Key findings from the present problem revealed that the velocity of the nanoliquid and hybrid nanofluid decreased due to greater nanoparticles volume fraction. Furthermore, the heat transportation is greater for mixed convection and thermophoresis parameter.

* Corresponding author.
** Corresponding author. Center of Excellence in Theoretical and Computational Science (TaCS-CoE), Science Laboratory Building, King Mongkut's University of Technology Thonburi (KMUTT), 126 Pracha-Uthit Road, Bang Mod, Thung Khru, Bangkok, 10140, Thailand.
E-mail addresses: poom.kum@kmutt.ac.th (P. Kumam), thidaporn.s@sciee.kmutnb.ac.th (T. Seangwattana).

https://doi.org/10.1016/j.heliyon.2023.e17678
Received 25 January 2023; Received in revised form 6 May 2023; Accepted 25 June 2023
Available online 26 June 2023

1. Introduction

Nanofluids can be prepared by mixing the different nanometer-sized particles such as nitride ceramics (*AIN*, *SIN*) semi-conductors (TiO_2, *SIC*), metals (*Cu*, *Ag*, *Au*), metallic oxides (Al_2O_3, *CuO*), and carbide ceramics (*SIC*, *TIC*) in the base liquid such as engine oil and water etc. In recent years, nanofluid has extensive range of applications in diverse fields of engineering, environmental and industrial processes such as solar-based science, cooling electronics, energy storage, heat exchangers, vehicle thermal applications, pharmaceuticals, food packing industry, cancer cells in human organs, bones, tissues, fiber artificial organs, automobiles, aviation, aerospace, power, energy, microelectronics fuels cells, lubrications, transportation, air-conditioning, and etc. Due to these applications of the nf, researchers have employed nanofluid in their fields of interest for the enhancement of heat transport. Siddique et al. [1] have revealed the investigation of entropic optimization and autocatalysis chemical reactions in a flow of *Cu*-water and Al_2O_3-water nanoliquid due to the stretched cylinder and obtained that the nanoliquid velocity is amplified for greater curvature parameter. Song et al. [2] have identified the role of the Williamson nanoliquid flow over an elongating cylinder including the psychical significance of the magnetic field. It has been pointed out that the increase in the thermophoretic factor increased the heat transference rate. Waqas et al. [3] have presented a study of the mixed convective stratified couple stress nanofluid along with the occurrence of heat flux due to the vertical exterior. It is noted that the increment in the buoyancy ratio factor has enlarged the motile microorganism profile. Ullah et al. [4] have dissected the significance of the melting heat conditions by using the Prandtl-Eyring nanoliquid flow due to the linear stretched surface with Joule heating and chemical reaction. It has been examined that the energy curve is heightened due to the enrichment of the Eckert number. Reddy et al. [5] have addressed the upshot of the chemical reaction on the nanoliquid flow over curved surface. They simulated their problem with the use of the ND-solver technique. Swain et al. [6] have examined the Casson fluid flow due to the stretchy surface with thermal radiation. Further, they have employed the concepts of the Buongiorno model for the computation of energy communication. Prabakaran et al. [7] have deliberated the thermal operation of the CNT/ Al_2O_3 nanofluid in water over the stretching surface by using the applications of the homotopy analysis technique. It has been distinguished that the intensification of the Richardson number improved the surface drag force. Ramzan et al. [8] have determined the comparative study of copper oxide *CuO* and Iron oxide Fe_3O_4 (II, III) in a Williamson nanoliquid flow with magnetic dipole effect and activation energy. It has been noted that the amplification in the Schmidt number intensified the mass conveyance. Some related studies concerned to the nanofluid flow exist in Refs. [9–13].

A hybrid nanoliquid is an extension of the nanoliquid. In a hybrid nanofluid, two dissimilar kinds of nanoparticles are mixed into the base liquid. It has been proved by different experiments that hybrid nanofluid (hnf) performs better than regular fluids. In the different arenas of industries and engineering, hybrid nanofluid has an extensive variety of applications such as solar cells, cooling devices, generators cooling, defense, microfluidics, medicals, nuclear systems cooling, transportation, naval structures, power production engines, etc. Inspired by the hybrid nanofluids' aforementioned uses, several studies have been reported. Assiri et al. [14] have employed the *GO* and *Ag* nanomaterials for the fluid model along the strained sheet with the applications of the Fourier law and Hall current. Kumbhakar and Nandi [15] have employed the slip conditions on the hnf flow past an extending sheet comprising *Cu* and Al_2O_3 nanoparticles. It has detected that the solutal Biot number has increased the Sherwood number. Raizah et al. [16] have explored the radiation impact on the heat transportation through the hnf flow. Further, they used the copper *Cu*, graphene oxide *GO*, and aluminum oxide Al_2O_3 nanoparticles in an Ethylene glycol base fluid during the simulation of their model. Mahmood et al. [17] have presented a study of hnf flow due to the heated stretched cylinder including the combined role of the heat source and suction effects. Further, *Cu*, Fe_3O_4, and SiO_2 are mixed up into the base fluid for the creation of the ternary hnf. Zainal et al. [18] have considered the physical aspects of hnf flow having copper *Cu*,and aluminum oxide Al_2O_3 nanoparticles. Further, they have analyzed that the magnetic field parameter enlarged the heat transport. Tuz Zohra et al. [19] have calculated the energy transference due to the hybrid nanoliquid flow induced by a rotating disc. In this study, *Ag* and *MgO* NPs are scattered to water, for the creation of the hnf. Shah et al. [20] have calculated the combination of copper *Cu* and titanium dioxide TiO_2 in a water base liquid due to the flow of the Prandtl hybrid nanoliquid model with motile microorganisms. They have initiate that the increase in the Lewis number declined the liquid solutal profile. Zhang et al. [21] have debated the magnetic field impact of the hnf flow towards an elastics surface along with the mixing of the tantalum and nickel nanoparticles and found that the velocity curve is higher for the Darcy forces. Furthermore, some important results and studies have been also presented by Refs. [22–26].

In various industrial, engineering, and natural processes, the phenomena of the chemical reaction (CR) have played a vital role. The main uses of the chemical reactions in different fields of industrial, technological, environmental and engineering processes are combustion and furnace, filtration, refrigeration metal spinning, erosion in iron, heat transportation, mass transportation, etc. Many researchers and scientist have employed chemical reaction in their fields of study because of their enormous variety of applications. Bilal et al. [27] described the fluid flow with influence of CR on the bioconvective hnf flow above the wedge and cone through the permeable media. They have obtained that the nanofluid temperature is greater in the case of radiation effect. Biswas et al. [28] have studied the prevalence of CR due to the nf flow across the elongating sheet. Reddy and Sreedevi [29] have computed the heat-mass transference and spotted that the rise in the radiation factor reduced the thermal profile. Shah et al. [30] have used the cross-nanofluid model with the physical aspects of thermal conductivity, and CR due to the cylindrical panels. In this investigation, they have found an increment in Sherwood's number due to CR factor. Bayones et al. [31] have considered the effects of CR across the nonlinear radiative Maxwell hnf flow by an elongating surface with Soret impacts. They have employed the similarity conversions for the renovation of highly PDEs into ODEs. Bilal et al. [32] have discussed the hybrid nanoliquid conveying small nanoparticles along the extending surface with Darcy forces. A numerical technique known as the bvp4c is used for the simulation of their model. Patil et al. [33] have used the convectively heated surface for the study of the CR on the Prandtl nanoliquid flow with the magnetic impact and initiated that the nanoliquid is amplified for greater Biot number. Ramzan et al. [34] have discoursed the uses of engine oil and autocatalytic CR due to the cross-hnf flow. In this study, graphene oxide *GO* and molybdenum disulfide SiO_2 are used as the nanoparticles.

Activation energy (AE) is process in which the minimum amount of the energy is required to initiate the chemical reaction process. In 1889, firstly the idea of the AE was revealed by Arrhenius. The activation energy has a lot of manufacturing and industrial uses such as oil reservoir, water emulsion, chemical engineering, food processing, liquid metal filtration, geothermal engineering, chemical reaction species, heat exchangers, fusion control, casting, heat transfer in heat media, nuclear reactors cooling, metallurgy, thermal magnetic flux, and many others. The scientists have presented a lot of models related to the activation energy under different geometrical configurations due to their widespread array of applications in different areas of industries and engineering. Azam et al. [35] have explored the numerical consequence of the activation energy on the radiative Casson nanoliquid flow with viscous dissipation along the moving cylinder. It has been determined that the motile number is reduced through the greater Peclet number. Habib et al. [36] have discussed the nanoliquid flow with activation energy and motile gyrotactic microorganism in which they obtained that the velocity curve is weakened for the greater rotating parameter. Ullah et al. [37] have employed Fourier law for the study of heat transport on the magnetized Prandtl-Eyring Powell hnf flow with melting heat transport and AE. The heightening in heat transference is noticed for the higher melting parameter. Sarkar et al. [38] scrutinized the energy and mass transition with entropy generation and non-Newtonian Viscoelastic nanofluid flowing over a stretching cylinder. Alsallami et al. [39] have used the rotating disk for the computation of activation energy and entropic generation due to the Marangoni Maxwell nanofluid flow. It has been obtained that the increase in temperature difference parameter increased the Bejan number. Li et al. [40] have employed convective conditions for the study of the double diffusion flow of hnf over the extending sheet with the existence of the AE. Abdal et al. [41] discussed the physical aspects of AE on the Maxwell and Williamson hnf flow over the stretched surface through the permeable medium. Ali et al. [42] focused on entropy generation's ascent in a MHD bioconvective slip flow of the nanoliquid comprising gyrotactic microbes over an elongated cylinder in the presence of AE. Some recent literature may be found in Refs. [43–45].

In view of the above-mentioned literature, it is noticed that the thermal conductivity of the common fluid has been improved by mixing the nano-particulates in the base fluid. The main goal of the present model is to discuss the heat and mass transport characteristics of the jet flow of hnf over the vertical stretching surface by using the idea of the heat source/sink, CR and AE. Further, the Brownian and thermophoresis diffusivity impacts are applied on the flow behavior. A hnf is designed by adding the cobalt ferrite $CoFe_2O_4$ and titanium dioxide TiO_2-NPs into the water H_2O base fluid. Through the application of the bvp4c technique in MATLAB, a numerical simulation of the present problem is performed. By using the graphs, the variation in velocity, energy, and mass is computed.

2. Mathematical formulation

We assumed the 2D Jet flow consists of nanoparticles across a vertical stretching surface. The hnf is produced by the scattering of hybrid Nano composites ($CoFe_2O_4$ and TiO_2). The following are some basic assumptions.

- The nanomaterials suspension is assumed to be diluted.
- Additionally, the consequences of second order CR and Arrhenius AE are considered.

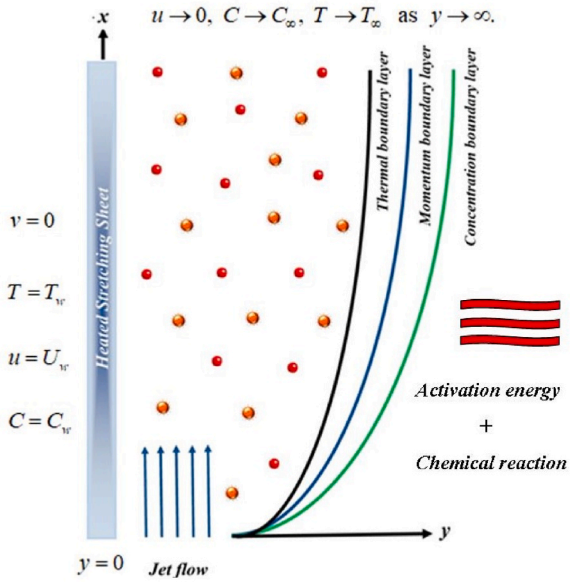

Fig. 1. Hybrid nanofluid flow across a stretching vertical surface [46].

- Two-dimensional jet flow.
- The effect of heat source is simulated with the energy equation.
- The sheet is stretching with uniform velocity U_w.
- The surface temperature and concentration is indicated by T_∞, C_∞, whereas T_w and C_w signifies the ambient as shown Fig. 1.

The mathematical framework takes the following arrangement [46,47]:

$$\frac{\partial u}{\partial x}+\frac{\partial v}{\partial y}=0, \tag{1}$$

$$u\frac{\partial u}{\partial x}+v\frac{\partial u}{\partial y}=\nu_{Tnf}\frac{\partial^2 u}{\partial y^2}-\frac{g}{\rho_{Tnf}}\left(\beta_t\rho_f(1-C_\infty)(T-T_\infty)-\beta_C\left(\rho_p-\rho_f\right)(C-C_\infty)\right), \tag{2}$$

$$u\frac{\partial T}{\partial x}+v\frac{\partial T}{\partial y}=\alpha_{Tnf}\frac{\partial^2 T}{\partial y^2}\left(D_B\frac{\partial T}{\partial y}\frac{\partial J}{\partial y}+\frac{D_T}{T_\infty}\left(\frac{\partial T}{\partial y}\right)^2\right)+\frac{Q_0}{(\rho c)_{Tnf}}(T-T_\infty), \tag{3}$$

$$u\frac{\partial C}{\partial x}+v\frac{\partial C}{\partial y}=D_B\frac{\partial^2 C}{\partial y^2}+\frac{D_T}{T_\infty}\frac{\partial T}{\partial y}-K_r^2(C-C_0)\left(\frac{T}{T_\infty}\right)^n\exp\left(-\frac{E_a}{\kappa T}\right), \tag{4}$$

Subjected to the boundary conditions (BCs) [46,47]:

$$\begin{aligned}&u=U_w, T=T_w, v=0, C=C_w \quad \text{at} \quad y=0,\\ &u\to 0, C\to C_\infty, T\to T_\infty \quad \text{as} \quad y\to\infty.\end{aligned} \tag{5}$$

here, the similarity transformations [46,47] and stream function ψ are expressed as

$$u=\frac{\partial\psi}{\partial y} \text{ and } v=\frac{-\partial\psi}{\partial x}.\psi=\left(\nu^2x\right)^{\frac{1}{4}}f, \Theta(\eta)=\frac{T-T_\infty}{T_w-T_\infty}, \Phi(\eta)=\frac{C-C_\infty}{C_w-C_\infty}, \eta=\frac{1}{4}\left(\nu^2x^3\right)^{\frac{-1}{4}}y. \tag{6}$$

By putting eq. (6) in eqs. (1)–(4) & eq. (5), we get:

$$\frac{\mu_{hnf}}{\mu_f}f'''+\frac{\rho_{hnf}}{\rho_f}\left(ff''-2f'^2\right)+64\lambda(\Theta-Nr\,\Phi)=0, \tag{7}$$

$$\frac{k_{hnf}}{k_f}\Theta''+\frac{\left(\rho C_p\right)_{hnf}}{\left(\rho C_p\right)_f}Pr\,f\Theta'+Nb\,\Theta'\,\Phi'+Nt\Theta'^2+Ht\Theta=0, \tag{8}$$

$$\Phi''+\frac{Nt}{Nb}\Theta''+ScF\Phi'-Kr(1+\varepsilon\delta)^n\Phi\ \exp\left(-\frac{E}{1+\varepsilon\delta}\right)=0, \tag{9}$$

The non-dimensional BCs are:

$$\begin{aligned}&f=0, f'=1, \Theta=1, \Phi=1 \quad \text{at} \quad y=0,\\ &f'\to 0, \Theta\to 0, \Phi\to 0 \quad \text{as} \quad y\to\infty.\end{aligned} \tag{10}$$

The skin friction, Nusselt number and Sherwood number are expressed as:

$$Cf_x=-\nu_{tnf}\frac{\left(\frac{\partial u}{\partial y}\right)_{y=0}}{U_w^2}, Nu_x=-\frac{xk_{tnf}}{k_f}\frac{\left(\frac{\partial T}{\partial y}\right)_{y=0}}{(T_w-T_\infty)}, Sh_x=-\frac{xD_B\left(\frac{\partial C}{\partial y}\right)_{y=0}}{(C_w-C_\infty)}. \tag{11}$$

The dimensionless form of eq. (11) are:

$$Cf_x=-\frac{\mu_{hnf}}{\mu_f}\frac{-f''(0)}{\sqrt{Re_x}}, \frac{Nu_x}{\sqrt{Re_x}}=-\frac{k_{hnf}}{k_f}\Theta'(0), \frac{Sh_x}{\sqrt{Re_x}}=-\Phi'(0). \tag{12}$$

The non-dimensional parameters are stated as:

Table 1
The experimental values of $(\varphi_1=\varphi_{TiO_2})$ and $(\varphi_3=\varphi_{CoFe_2O_4})$ [48].

Base fluid & Nanoparticles	$\rho(\text{kg}/\text{m}^3)$	$k(\text{W}/\text{mK})$	$Cp(j/kgK)$	$\sigma(S/m)$
H_2O	997.1	0.613	4179	0.05
TiO_2	4250	8.953	686.2	2.38×10^6
$CoFe_2O_4$	4907	3.7	700	5.51×10^9

$$\lambda = \frac{g\beta_T(T_w - T_\infty)(1 - C_\infty)}{\nu_f}, Nt = \frac{D_T(\rho C_p)_{hnf}(T_w - T_\infty)}{(\rho C_p)_f T_\infty \nu_f}, Nr = \frac{\beta_J(\rho_p - \rho_f)(C_w - C_\infty)}{\rho_f \beta_T (T_w - T_\infty)(1 - C_\infty)},$$
$$Nb = \frac{D_B(C_w - C_\infty)(\rho C_p)_{hnf}}{(\rho C_p)_f \nu_f}, \alpha_{hnf} = \frac{k_{hnf}}{(\rho C_p)_{hnf}}, Pr = \frac{\nu_f}{\alpha_f}, Sc = \frac{\alpha_f}{D_B}, E = \frac{E_a}{\kappa T_\infty}, Kr = \frac{K_r^2}{\nu_f}. \tag{13}$$

Tables 1 and 2 illustrate the experimental values and mathematical model used for the estimation of the hybrid nanoliquid as given as.

3. Numerical solution

The reduced obtained set of ODEs (7)–(9) and (10) are solved by using Matlab built-in package bvp4c. For the purposed, the set of ODEs are further simplified to 1st order differential equations by employing the following variables.

$$\Im_1 = f(\eta), \Im_2 = f'(\eta), \Im_3 = f''(\eta), \Im_4 = \Theta(\eta), \Im_5 = \Theta'(\eta), \Im_6 = \Phi(\eta), \Im_7 = \Phi'(\eta). \tag{14}$$

By incorporating eq. (14) in eqs. (7)–(10), we get:

$$\frac{\mu_{hnf}}{\mu_f}\Im_3' + \frac{\rho_{hnf}}{\rho_f}\left(\Im_1\Im_3 - 2\Im_2^{\,2}\right) + 64\lambda(\Im_4 - Nr\Im_6) = 0, \tag{15}$$

$$\frac{k_{hnf}}{k_f}\Im_5' + \frac{(\rho C_p)_{hnf}}{(\rho C_p)_f} Pr\,\Im_1\Im_5 + Nb\Im_5\Im_7 + Nt\Im_5^{\,2} + Ht\Im_4 = 0, \tag{16}$$

$$\Im_7' + \frac{Nt}{Nb}\Im_5' + Sc\,\Im_1\Im_7 - (1 + \varepsilon\delta)^n Kr\,\Im_6\,\exp\left(-\frac{E}{1 + \varepsilon\delta}\right) = 0, \tag{17}$$

The BCs are:

$$\left.\begin{array}{l} \Im_1 = 0, \Im_2 = 1, \Im_4 = 1, \Im_6 = 1 \quad \text{at} \quad y = 0, \\ \Im_2 \to 0, \Im_4 \to 0, \Im_6 \to 0 \quad \text{as} \quad y \to \infty. \end{array}\right\} \tag{18}$$

The obtained set of Eq. (15)–(18) are further solved through Matlab software using bvp4c package.

4. Results and discussion

In this part, the physical significance of the chemically reacting jet flow of mixed convection hnf with AE and CR is elaborated. For simulation, the higher order ODEs (7–9) along boundary condition (10) are solved by using the numerical built-in bvp4c technique in MATLAB. Further, the effects of the involved flow constraints on the velocity, energy, and concentration of the nanofluid (nf) and hnf are demonstrated in a graphical form.

Figs. 2–4 are drawn to find out the physical implication of the *Nr*, φ and λ on the velocity of the CoF_2O_4/water nf and $TiO_2 + CoF_2O_4$/water hnf. The impact of the *Nr* on the velocity of the CoF_2O_4/water nf and $TiO_2 + CoF_2O_4$/water hnf is examined in Fig. 2. It has been analyzed that the velocity of the fluid drops when the *Nr* amplifies. Physically, it is detected that when the *Nr* increases that

Table 2
The mathematical model of hybrid nanoliquid ($\varphi_1 = \varphi_{MgO}, \varphi_2 = \varphi_{CoFe_2O_4}$) [49].

Properties	Models
Viscosity	$\frac{\mu_{hnf}}{\mu_{bf}} = \frac{1}{(1 - \varphi_{TiO_2} - \varphi_{CoFe_2O_4})^2}$
Density	$\frac{\rho_{hnf}}{\rho_{bf}} = \varphi_{TiO_2}\left(\frac{\rho_{TiO_2}}{\rho_{bf}}\right) + \varphi_{CoFe_2O_4}\left(\frac{\rho_{CoFe_2O_4}}{\rho_{bf}}\right) + (1 - \varphi_{TiO_2} - \varphi_{CoFe_2O_4})$
Thermal Capacity	$\frac{(\rho C_p)_{hnf}}{(\rho C_p)_{bf}} = \varphi_{TiO_2}\left(\frac{(\rho C_p)_{TiO_2}}{(\rho C_p)_{bf}}\right) + \varphi_{CoFe_2O_4}\left(\frac{(\rho C_p)_{CoFe_2O_4}}{(\rho C_p)_{bf}}\right) + (1 - \varphi_{TiO_2} - \varphi_{CoFe_2O_4})$
Thermal Expansion	$\frac{(\rho \beta_T)_{hnf}}{(\rho \beta_T)_{bf}} = \varphi_{TiO_2}\left(\frac{(\rho \beta_T)_{TiO_2}}{(\rho \beta_T)_{bf}}\right) + \varphi_{CoFe_2O_4}\left(\frac{(\rho \beta_T)_{CoFe_2O_4}}{(\rho \beta_T)_{bf}}\right) + (1 - \varphi_{TiO_2} - \varphi_{CoFe_2O_4})$
Thermal Conductivity	$\frac{k_{hnf}}{k_{bf}} = \left[\frac{\left(\frac{\varphi_{TiO_2}k_{TiO_2} + \varphi_{CoFe_2O_4}k_{CoFe_2O_4}}{\varphi_{TiO_2} + \varphi_{CoFe_2O_4}}\right) + 2k_{bf} + 2(\varphi_{TiO_2}k_{TiO_2} + \varphi_{CoFe_2O_4}k_{CoFe_2O_4}) - 2(\varphi_{TiO_2} + \varphi_{CoFe_2O_4})k_{bf}}{\left(\frac{\varphi_{TiO_2}k_{TiO_2} + \varphi_{CoFe_2O_4}k_{CoFe_2O_4}}{\varphi_{TiO_2} + \varphi_{CoFe_2O_4}}\right) + 2k_{bf} - 2(k_{TiO_2}\varphi_{TiO_2} + k_{CoFe_2O_4}\varphi_{CoFe_2O_4}) + 2(\varphi_{TiO_2} + \varphi_{CoFe_2O_4})k_{bf}}\right]$
Electrical Conductivity	$\frac{\sigma_{hnf}}{\sigma_{bf}} = \left[\frac{\left(\frac{\varphi_{TiO_2}\sigma_{TiO_2} + \sigma_{CoFe_2O_4}\varphi_{CoFe_2O_4}}{\varphi_{CoFe_2O_4} + \varphi_{TiO_2}}\right) + 2\sigma_{bf} + 2(\varphi_{TiO_2}\sigma_{TiO_2} + \varphi_{CoFe_2O_4}\sigma_{CoFe_2O_4}) - 2(\varphi_{TiO_2} + \varphi_{CoFe_2O_4})\sigma_{bf}}{\left(\frac{\varphi_{TiO_2}\sigma_{TiO_2} + \varphi_{CoFe_2O_4}\sigma_{CoFe_2O_4}}{\varphi_{TiO_2} + \varphi_{CoFe_2O_4}}\right) + 2\sigma_{bf} - (\varphi_{TiO_2}\sigma_{TiO_2} + \varphi_{CoFe_2O_4}\sigma_{CoFe_2O_4}) + (\varphi_{TiO_2} + \varphi_{CoFe_2O_4})\sigma_{bf}}\right]$

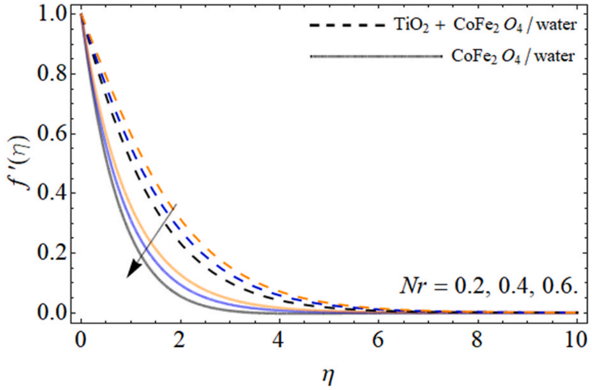

Fig. 2. Effect of thermophoresis parameter *Nr* on the velocity $f'(\eta)$ curve.

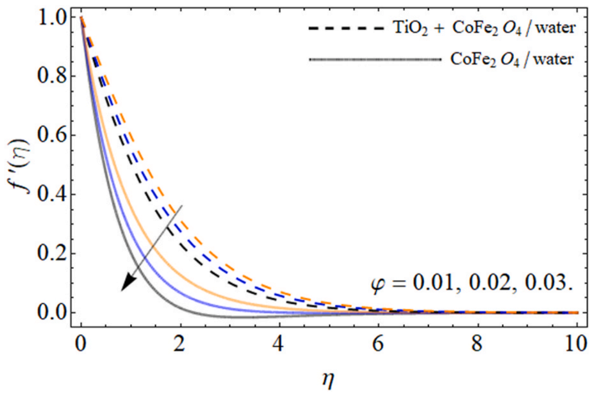

Fig. 3. Effect of nanocomposites φ on the velocity curve $f'(\eta)$.

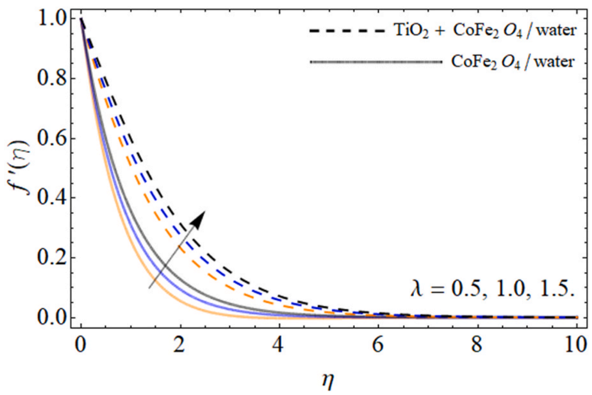

Fig. 4. Effect of mixed convection parameter λ on the velocity $f'(\eta)$ curve.

resist the fluid motion because the *Nr* is related to the buoyancy forces. Therefore, the velocity of the CoF_2O_4/water nf and $TiO_2 + CoF_2O_4$/water hnf is reduces. Fig. 3 signifies the variation of the velocity of the CoF_2O_4/water nanoliquid and $TiO_2 + CoF_2O_4$/water hnf against higher values of the φ. In this enquiry, decreasing behavior of the velocity is observed due to the change of φ. By increasing φ, the viscosity of the nf and hnf is increases which is the key factor that decrease the velocity of the CoF_2O_4/water nf and $TiO_2 + CoF_2O_4$/water hnf.

Fig. 4 capture the flow pattern of the velocity of the CoF_2O_4/water nf and $TiO_2 + CoF_2O_4$/water hnf due to the augmentation of λ. For varying values of λ, the velocity of the CoF_2O_4/water nf and $TiO_2 + CoF_2O_4$/water hnf is amplifies. The effects of the *Nb*, *Nt*, φ and *Ht* on the temperature of the CoF_2O_4/water nf and $TiO_2 + CoF_2O_4$/water hnf is scrutinized in Figs. 5–8. The variation in the temperature of the CoF_2O_4/water nf and $TiO_2 + CoF_2O_4$/water hnf versus amplifying values of the *Nb* is considered in Fig. 5. Fig. 5 exposed

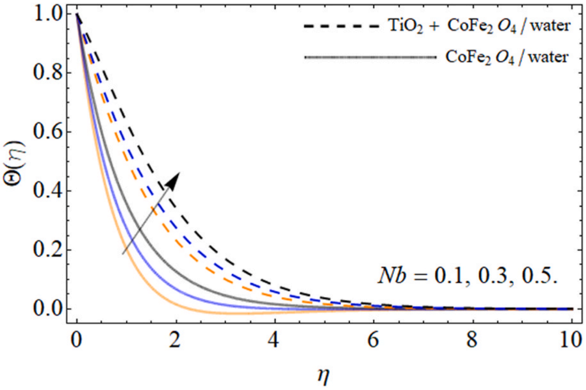

Fig. 5. Effect of Brownian motion factor *Nb* on the energy $\theta(\eta)$ curve.

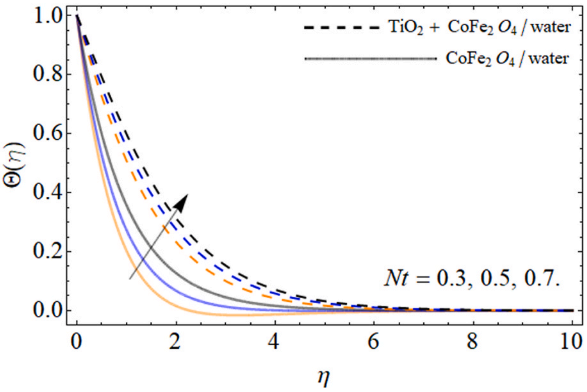

Fig. 6. Effect thermophoresis parameter *Nt* on the energy curve $\theta(\eta)$.

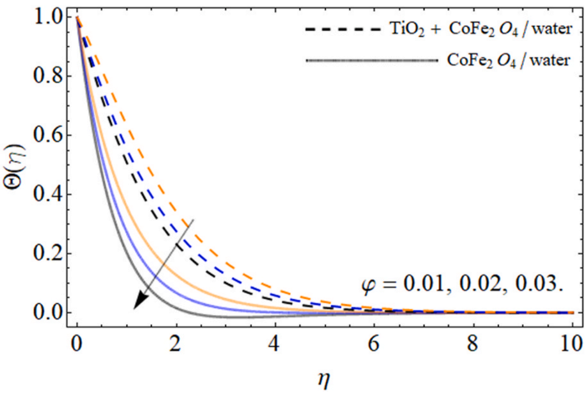

Fig. 7. Effect of nanoparticles φ on the energy curve $\theta(\eta)$.

that the intensification in *Nb* amplifies the energy of the CoF_2O_4/water nf and $TiO_2 + CoF_2O_4$/water hnf. The increase of *Nb* (i.e. the increase of the concentration of nanoparticles in a fluid) causes an intensification in the rate of energy transference between the fluid and the nanoparticles. This is due to the enhanced thermal boundary resistance between the fluid and the nanoparticles, caused by the increased collisions between the fluid molecules and the nanoparticles. This increased heat transfer results in a higher temperature amplitude in the nanofluid.

Fig. 6 is presented to access the fluctuation in the temperature of the CoF_2O_4/water nf and $TiO_2 + CoF_2O_4$/water hnf for greater estimates of the thermophoresis parameter *Nt*. This graph explains that the magnitude of the temperature of the CoF_2O_4/water nf and $TiO_2 + CoF_2O_4$/water hnf is rises when the *Nt* is grown up. Nanofluids are suspensions of nanoparticles in a liquid, and the thermophoresis parameter is a measure of the ability of the nanoparticles to transfer in response to temperature gradient. As the

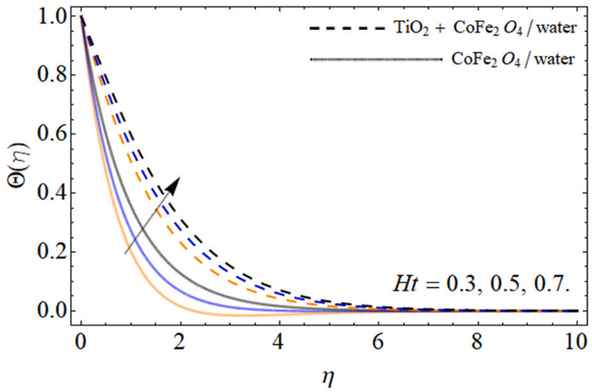

Fig. 8. Effect of heat source *Ht* on the energy curve $\theta(\eta)$.

thermophoresis parameter increases, the nanoparticles are more likely to move towards regions of higher temperature, which can lead to an upsurge in the temperature. This is because the nanoparticles are able to transport heat more effectively, leading to a more efficient transfer of thermal energy throughout the fluid. Additionally, the increased motion of the nanoparticles can also enhance the mixing of the nanofluid, which can also contribute to an increase in temperature.

In Fig. 7, the change in the temperature of the CoF_2O_4/water nf and $TiO_2 + CoF_2O_4$/water hnf with respect to the higher nanoparticle volume fraction φ is explained. It is seeming that the intensifying values of nanoparticle φ decays the temperature of the CoF_2O_4/water nf and $TiO_2 + CoF_2O_4$/water hnf. Fig. 8 is plotted to determine the physical role of the *Ht* on the energy of the CoF_2O_4/water nf and $TiO_2 + CoF_2O_4$/water hnf. In this observation, it is elaborated that the increase in *Ht* increased the energy curve. The increase of heat generation factor (i.e. the increase of the rate of heat generation within the nanoparticles) causes an increase in the overall temperature. This is because the heat generated within the nanoparticles is transferred to the fluid via radiation, conduction and convection. As the heat generation rate increases, more heat is transported to the fluid, resulting in a higher energy curve. Additionally, the increased heat generation rate can also cause the temperature of the nanoparticles to increase, which can lead to further heat transfer to the fluid and further temperature amplification.

Figs. 9–11 are sketched to discuss the role of *E*, *Kr* and *Sc* on the concentration of the CoF_2O_4/water nf and $TiO_2 + CoF_2O_4$/water hnf. The impact of the activation energy factor *E* on the concentration of the CoF_2O_4/water nf and $TiO_2 + CoF_2O_4$/water hnf is evaluated in Fig. 9. In this analysis, an increment in the concentration of the CoF_2O_4/water nf and $TiO_2 + CoF_2O_4$/water hnf is observed for the higher *E*. It has noted that with the upsurging of the AE term *E*, the modified Arrhenius function is deprecating which consequently favor in the chemical reaction production.

Fig. 10 has displayed the increasing role of *Kr* on the concentration of the CoF_2O_4/water nf and $TiO_2 + CoF_2O_4$/water hnf. It is seen that the concentration of the CoF_2O_4/water nf and $TiO_2 + CoF_2O_4$/water hnf is diminishes when the chemical reaction parameter *Kr* is enhances. It is examined that the mass transmission rate is amplifies but the thickness of the concentration boundary layer is lower when the *Kr* is augmented. As a result, concentration of the CoF_2O_4/water nf and $TiO_2 + CoF_2O_4$/water hnf is weakens when the *Kr* is enhances. The change in the concentration of the CoF_2O_4/water nf and $TiO_2 + CoF_2O_4$/water hnf due to the various values of the *Sc* is determined in Fig. 11. In this Fig. 11, the declines behavior of the concentration of the CoF_2O_4/water nf and $TiO_2 + CoF_2O_4$/water hnf is examined with respect to higher *Sc*. The molecular diffusivity of the nf and hnf is diminished which consequently declines the concentration of the CoF_2O_4/water nf and $TiO_2 + CoF_2O_4$/water hnf. Because *Sc* and molecular diffusivity are inversely proportional to each other. Therefore, with the increase of *Sc* the molecular diffusivity is reduces. So, the concentration becomes higher for both nanofluid and hybrid when the *Sc* is higher.

Table 3 is presented to analyze the physical significance of Cf_x, Sherwood number Sh_x and Nusselt number Nu_x versus φ, λ, *Nb*, *Nt*, and *Sc*. In this Table, it is predicted that the Cf_x is lower for higher mixed convection parameter λ, *Nb*,and *Sc*. Further, the amplifying role of the Cf_x is noticed due to the change in φ and *Nt*. Also, it is perceived that the increment in λ, *Nt*, and *Sc* led to intensify the Nusselt number Nu_x but the Nu_x is lower for higher φ, and *Nb*. Furthermore, Table 3 signifies that the Sherwood number Sh_x is increases due to the escalation of the φ, *Nt*, *Nb* and *Sc* but the declines role of the Sherwood number Sh_x is found for the greater λ. Table 4 particularizes the relative evaluation of the published literature with the present conclusions for the values of $-\theta'(0)$. The outcomes revealed that the present outcomes are accurate and reliable.

5. Conclusion

In this article, the thermal performance of the mixed convection flow of the hybrid nanofluid past a vertical stretching surface with the mixing of the cobalt ferrite $CoFe_2O_4$ and titanium dioxide TiO_2 nanoparticles into the water H_2O base fluid is studied. Further, the Brownian and thermophoresis diffusivity is discussed in the existing problem. For the numerical solution, the bvp4c technique in MATLAB is hired. Key findings of the present study are:

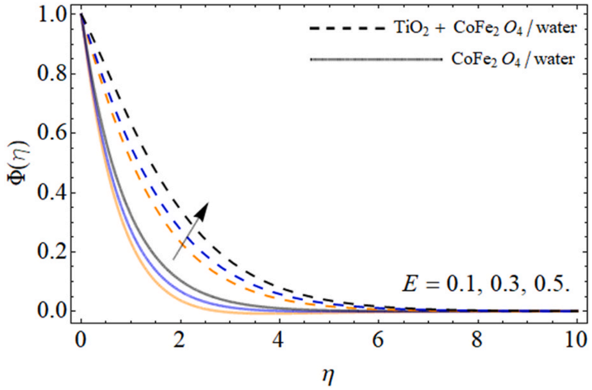

Fig. 9. Effect of Activation energy E on the concentration curve $\varphi(\eta)$.

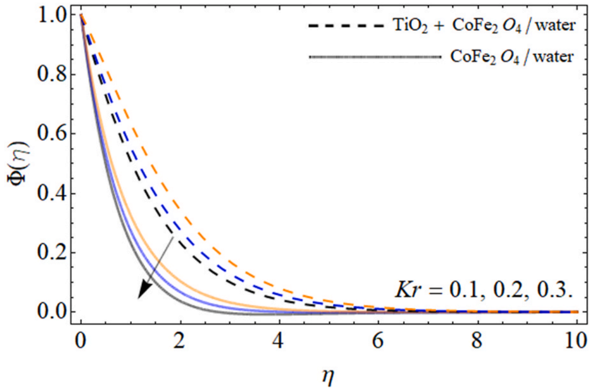

Fig. 10. Effect of chemical reaction Kr on the concentration curve $\varphi(\eta)$.

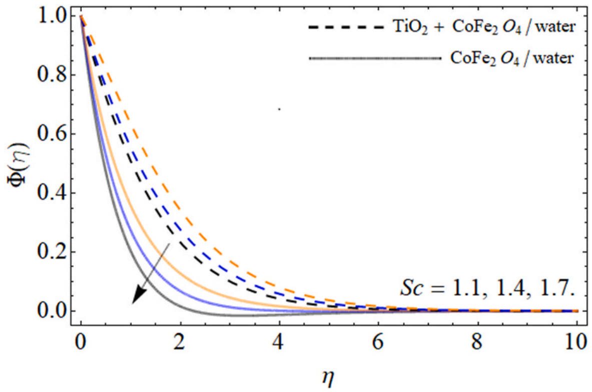

Fig. 11. Effect of Schmidth number Sc on the concentration curve $\varphi(\eta)$.

- Rise in nanoparticle quantities and thermophoresis parameter have increased the skin friction coefficient but the λ, Nb and Sc have declined the skin friction coefficient.
- Nusselt number is upsurges for the higher λ, thermophoresis parameter and Schmidt number but the Nusselt number is lower for greater Brownian motion parameter and nanoparticle volume fraction.
- A decaying role of Sherwood number is scrutinized for mixed convection parameter. Further, it is noticed that the Sherwood number is improves for the flourishing numbers of nanoparticle, thermophoresis and Brownian diffusion and Schmidt number.
- It is detected that the higher values of λ cause to increase the velocity of the nf and hnf. Moreover, the velocity of the nanofluid and hnf is lessened due to buoyancy ratio parameter and nanoparticle volume fraction.

Table 3
Numerical results for Nusselt number, skin friction and Sherwood number.

Parameter	Values	Cf_x	Nu_x	Sh_x
φ	0.01	0.22885615	0.41387465	1.07947700
	0.02	0.28274785	0.38679763	1.11174585
	0.03	0.25159785	0.35845469	1.10366863
λ	0.0	0.75907118	0.13369625	1.11710182
	0.2	0.72975841	0.13883824	1.10003878
	0.4	0.70223339	0.14300426	1.10262520
Nt	1.0	0.31540593	0.34518183	1.11680600
	2.0	0.31631817	0.23652449	1.21480310
	3.0	0.31640133	0.15818906	1.38548408
Nb	1.0	0.31456575	0.31387465	0.77671954
	2.0	0.31203913	0.21975442	0.88787082
	3.0	0.31038548	0.11033907	1.15276029
Sc	0.5	0.32007475	0.36836995	0.66609049
	1.0	0.31456575	0.31387465	1.08747700
	1.5	0.31216768	0.38619710	1.39801025

Table 4
The relative comparison of the published literature with the present outcomes.

Parameter	Khan and Pop [50]	Wang [51]	Puneeth [46]	Present work
Pr	$-\theta'(0)$	$-\theta'(0)$	$-\theta'(0)$	$-\theta'(0)$
0.07	0.066	0.066	0.066	0.06621
0.20	0.169	0.169	0.169	0.16932
0.70	0.454	0.454	0.454	0.45464
2.00	0.911	0.911	0.911	0.91162

- ❖ Nanoliquid and hybrid nanofluid temperature is greater for the higher Brownian motion parameter, thermophoresis parameter, and heat generation parameter. Further, the nanofluid and hybrid nanofluid temperature show decreasing behavior for the nanoparticles volume fraction.
- ❖ Enhancement in activation energy parameter amplified the concentration of the nanofluid and hybrid nanofluid but intensification in chemical reaction factor and Schmidt number have declined the concentration of the nanofluid and hybrid nanofluid.
- ❖ The proposed model may be extended by considering several physical effects and different boundary conditions, and can be solved for trihybrid nanofluid using other numerical, analytical and fractional techniques.

Funding information

The authors acknowledge the financial support provided by the Center of Excellence in Theoretical and Computational Science (TaCS-CoE), KMUTT. This research was funded by National Science, Research and Innovation Fund (NSRF), King Mongkut's University of Technology North Bangkok with Contract no. KMUTNB–FF–66-36.

Author contribution statement

Nidhish Kumar Mishra:Analyzed and interpreted the data; Wrote the paper.
Sadia Anwar, Anwar Saeed: Conceived and designed the analysis.
Poom Kumam: Contributed analysis tools or data; Wrote the paper.
Thidaporn Seangwattana: Analyzed and interpreted the data.
Muhammad Bilal: Contributed analysis tools or data.

Data availability statement

Data will be made available on request.

Declaration of competing interest

The authors declare that they have no known competing financial interests or personal relationships that could have appeared to influence the work reported in this paper.

Nomenclatures

Stream function ψ
Two-dimensional 2D
Specific heat $JKgK^{-1}$ C_p
Arrhenius activation energy E_a
Density Kgm^{-3} ρ
Thermal conductivity $(W/m.K)$ k_{hnf}
Reynold number Re_x
Rayleigh number Rb
Nusselt number Nu_x
Nanoparticles volume friction φ
Brownian motion Nb
Schmidth number Sc
Lewies number Sb
Aluminum oxide Al_2O_3
Peclet number Pe
Temperature at free stream $[K]$ T_∞
Stretching velocity (m/s) U_w.
Heat source Q_0
Chemical reaction K_r^2
Thermal radiation Nr
Dynamic viscosity $Kgm^{-1}s^{-1}$ μ
Mixed convection factor λ
Electrical conductivity (S/m) σ_{hnf}
Heat source term hs
Sherwood number Sh_x
Thermophoresis term Nt
Skin friction Cf
Cobalt ferrite $CoFe_2O_3$
Titanium dioxide TiO_2
Parametric continuation method PCM

References

[1] B.K. Siddiqui, S. Batool, Q. mahmood ul Hassan, M.Y. Malik, Repercussions of homogeneous and heterogeneous reactions of 3D flow of Cu-water and AL2O3-water nanofluid and entropy generation estimation along stretching cylinder, Ain Shams Eng. J. 13 (1) (2022), 101493.
[2] Y.Q. Song, A. Hamid, T.C. Sun, M.I. Khan, S. Qayyum, R.N. Kumar, R. Chinram, Unsteady mixed convection flow of magneto-Williamson nanofluid due to stretched cylinder with significant non-uniform heat source/sink features, Alex. Eng. J. 61 (1) (2022) 195–206.
[3] H. Waqas, A. Wakif, Q. Al-Mdallal, M. Zaydan, U. Farooq, M. Hussain, Significance of magnetic field and activation energy on the features of stratified mixed radiative-convective couple-stress nanofluid flows with motile microorganisms, Alex. Eng. J. 61 (2) (2022) 1425–1436.
[4] I. Ullah, R. Ali, H. Nawab, I. Uddin, T. Muhammad, I. Khan, K.S. Nisar, Theoretical analysis of activation energy effect on Prandtl–Eyring nanoliquid flow subject to melting condition, J. Non-Equilibrium Thermodyn. 47 (1) (2022) 1–12.
[5] S.C. Reddy, K.K. Asogwa, M.F. Yassen, Z. Adnan, Z. Iqbal, M-Eldin, . Sayed, K.M. Swarnalatha, Dynamics of MHD second-grade nanofluid flow with activation energy across a curved stretching surface, Front. Energy Res. 10 (2022).
[6] K. Swain, M. Mishra, A. Kumari, Numerical study of Casson nanofluid over an elongated surface in presence of Joule heating and viscous dissipation: Buongiorno model analysis, J. Comput. Appl. Mech. 53 (3) (2022) 414–430.
[7] R. Prabakaran, S. Eswaramoorthi, K. Loganathan, I.E. Sarris, Investigation on thermally radiative mixed convective flow of carbon nanotubes/Al 2 O 3 nanofluid in water past a stretching plate with joule heating and viscous dissipation, Micromachines 13 (9) (2022) 1424.
[8] M. Ramzan, S. Rehman, M.S. Junaid, A. Saeed, P. Kumam, W. Watthayu, Dynamics of Williamson Ferro-nanofluid due to bioconvection in the portfolio of magnetic dipole and activation energy over a stretching sheet, Int. Commun. Heat Mass Tran. 137 (2022), 106245.
[9] N.A. Shah, A. Wakif, E.R. El-Zahar, S. Ahmad, S.J. Yook, Numerical Simulation of a Thermally Enhanced EMHD Flow of a Heterogeneous Micropolar Mixture Comprising (60%)-ethylene Glycol (EG),(40%)-water (W), and Copper Oxide Nanomaterials (CuO), Case Studies in Thermal Engineering, 2022, 102046.
[10] A. Ali, S. Sarkar, S. Das, Bioconvective chemically reactive entropy optimized Cross-nano-material conveying oxytactic microorganisms over a flexible cylinder with Lorentz force and Arrhenius kinetics, Math. Comput. Simulat. 205 (2023) 1029–1051.
[11] S. Sarkar, S. Das, Magneto-thermo-bioconvection of a chemically sensitive Cross nanofluid with an infusion of gyrotactic microorganisms over a lubricious cylindrical surface: statistical analysis, Int. J. Model. Simulat. (2022) 1–22.
[12] F.T. Zohra, M.J. Uddin, A.I. Ismail, Magnetohydrodynamic bio-nanoconvective Naiver slip flow of micropolar fluid in a stretchable horizontal channel, Heat Tran. Asian Res. 48 (8) (2019) 3636–3656.
[13] N.A. Latiff, M.J. Uddin, A.M. Ismail, Stefan blowing effect on bioconvective flow of nanofluid over a solid rotating stretchable disk, Propulsion and power research 5 (4) (2016) 267–278.
[14] T.A. Assiri, F.A. Aziz Elsebaee, A.M. Alqahtani, M. Bilal, A. Ali, S.M. Eldin, Numerical simulation of energy transfer in radiative hybrid nanofluids flow influenced by second-order chemical reaction and magnetic field, AIP Adv. 13 (3) (2023), 035020.
[15] B. Kumbhakar, S. Nandi, Unsteady MHD radiative-dissipative flow of Cu-Al2O3/H2O hybrid nanofluid past a stretching sheet with slip and convective conditions: a regression analysis, Math. Comput. Simulat. 194 (2022) 563–587.

[16] Z. Raizah, A. Saeed, M. Bilal, A.M. Galal, E. Bonyah, Parametric simulation of stagnation point flow of motile microorganism hybrid nanofluid across a circular cylinder with sinusoidal radius, Open Phys. 21 (1) (2023), 20220205.
[17] Z. Mahmood, Z. Iqbal, M.A. Alyami, B. Alqahtani, M.F. Yassen, U. Khan, Influence of suction and heat source on MHD stagnation point flow of ternary hybrid nanofluid over convectively heated stretching/shrinking cylinder, Adv. Mech. Eng. 14 (9) (2022), 16878132221126278.
[18] N.A. Zainal, R. Nazar, K. Naganthran, I. Pop, Magnetic impact on the unsteady separated stagnation-point flow of hybrid nanofluid with viscous dissipation and joule heating, Mathematics 10 (13) (2022) 2356.
[19] F. Tuz Zohra, M.J. Uddin, M.F. Basir, A.I.M. Ismail, Magnetohydrodynamic bio-nano-convective slip flow with Stefan blowing effects over a rotating disc, Proc. Inst. Mech. Eng., Part N: Journal of Nanomaterials, Nanoengineering and Nanosystems 234 (3–4) (2020) 83–97.
[20] S.A.A. Shah, N.A. Ahammad, E.M.T.E. Din, F. Gamaoun, A.U. Awan, B. Ali, Bio-convection effects on Prandtl hybrid nanofluid flow with chemical reaction and motile microorganism over a stretching sheet, Nanomaterials 12 (13) (2022) 2174.
[21] L. Zhang, M.M. Bhatti, E.E. Michaelides, M. Marin, R. Ellahi, Hybrid nanofluid flow towards an elastic surface with tantalum and nickel nanoparticles, under the influence of an induced magnetic field, Eur. Phys. J.: Spec. Top. 231 (3) (2022) 521–533.
[22] N.A. Latiff, M.J. Uddin, A.M. Ismail, Stefan blowing effect on bioconvective flow of nanofluid over a solid rotating stretchable disk, Propulsion and power research 5 (4) (2016) 267–278.
[23] M.J. Uddin, O.A. Bég, A.I. Ismail, Radiative convective nanofluid flow past a stretching/shrinking sheet with slip effects, J. Thermophys. Heat Tran. 29 (3) (2015) 513–523.
[24] N.A. Amirsom, M.J. Uddin, M.F.M. Basir, A.I.M. Ismail, O.A. Bég, A. Kadir, Three-dimensional bioconvection nanofluid flow from a bi-axial stretching sheet with anisotropic slip, Sains Malays. 48 (5) (2019) 1137–1149.
[25] M. Ramzan, S. Riasat, S.F. Aljurbua, H.A.S. Ghazwani, O. Mahmoud, Hybrid nanofluid flow induced by an oscillating disk considering surface catalyzed reaction and nanoparticles shape factor, Nanomaterials 12 (11) (2022) 1794.
[26] M.J. Babu, Y.S. Rao, A.S. Kumar, C.S.K. Raju, S.A. Shehzad, T. Ambreen, N.A. Shah, Squeezed flow of polyethylene glycol and water based hybrid nanofluid over a magnetized sensor surface: a statistical approach, Int. Commun. Heat Mass Tran. 135 (2022), 106136.
[27] M. Bilal, I. Ullah, M.M. Alam, W. Weera, A.M. Galal, Numerical simulations through PCM for the dynamics of thermal enhancement in ternary MHD hybrid nanofluid flow over plane sheet, cone, and wedge, Symmetry 14 (11) (2022) 2419.
[28] R. Biswas, M.S. Hossain, R. Islam, S.F. Ahmmed, S.R. Mishra, M. Afikuzzaman, Computational treatment of MHD Maxwell nanofluid flow across a stretching sheet considering higher-order chemical reaction and thermal radiation, Journal of Computational Mathematics and Data Science 4 (2022), 100048.
[29] P. Sudarsana Reddy, P. Sreedevi, Impact of chemical reaction and double stratification on heat and mass transfer characteristics of nanofluid flow over porous stretching sheet with thermal radiation, Int. J. Ambient Energy 43 (1) (2022) 1626–1636.
[30] S.L. Shah, A. Ayub, S. Dehraj, H.A. Wahab, K.M. Sagayam, M.R. Ali, Z. Sabir, Magnetic dipole aspect of binary chemical reactive Cross nanofluid and heat transport over composite cylindrical panels, Waves Random Complex Media (2022) 1–24.
[31] F.S. Bayones, A.M. Abd-Alla, E.N. Thabet, Magnetized Dissipative Soret Effect on Nonlinear Radiative Maxwell Nanofluid Flow with Porosity, Chemical Reaction and Joule Heating, Waves in Random and Complex Media, 2022, pp. 1–19.
[32] M. Bilal, F.S. Alduais, H. Alrabaiah, A. Saeed, Numerical evaluation of Darcy Forchhemier hybrid nanofluid flow under the consequences of activation energy and second-order chemical reaction over a slender stretching sheet, Waves Random Complex Media (2022) 1–16.
[33] A.B. Patil, P.P. Humane, V.S. Patil, G.R. Rajput, MHD Prandtl nanofluid flow due to convectively heated stretching sheet below the control of chemical reaction with thermal radiation, Int. J. Ambient Energy (2021) 1–13.
[34] M. Ramzan, U. Shamshad, S. Rehman, M.S. Junaid, A. Saeed, P. Kumam, Analytical simulation of Hall current and cattaneo–christov heat flux in cross-hybrid nanofluid with autocatalytic chemical reaction: an engineering application of engine oil, Arabian J. Sci. Eng. (2022) 1–21.
[35] M. Azam, T. Xu, M.K. Nayak, W.A. Khan, M. Khan, Gyrotactic microorganisms and viscous dissipation features on radiative Casson nanoliquid over a moving cylinder with activation energy, Waves Random Complex Media (2022) 1–23.
[36] D. Habib, N. Salamat, S. Abdal, I. Siddique, M.C. Ang, A. Ahmadian, On the role of bioconvection and activation energy for time dependent nanofluid slip transpiration due to extending domain in the presence of electric and magnetic fields, Ain Shams Eng. J. 13 (1) (2022), 101519.
[37] Z. Ullah, I. Ullah, G. Zaman, T.C. Sun, A Numerical Approach to Interpret Melting and Activation Energy Phenomenon on the Magnetized Transient Flow of Prandtl–Eyring Fluid with the Application of Cattaneo–Christov Theory, Waves in Random and Complex Media, 2022, pp. 1–21.
[38] S. Sarkar, R.N. Jana, S. Das, Activation energy impact on radiated magneto-Sisko nanofluid flow over a stretching and slipping cylinder: entropy analysis, Multidiscip. Model. Mater. Struct. 16 (5) (2020) 1085–1115.
[39] S.A. Alsallami, H. Zahir, T. Muhammad, A.U. Hayat, M.R. Khan, A. Ali, Numerical simulation of Marangoni Maxwell nanofluid flow with Arrhenius activation energy and entropy anatomization over a rotating disk, Waves Random Complex Media (2022) 1–19.
[40] Y.X. Li, U.F. Alqsair, K. Ramesh, S.U. Khan, M.I. Khan, Nonlinear heat source/sink and activation energy assessment in double diffusion flow of micropolar (non-Newtonian) nanofluid with convective conditions, Arabian J. Sci. Eng. 47 (1) (2022) 859–866.
[41] S. Abdal, I. Siddique, D. Alrowaili, Q. Al-Mdallal, S. Hussain, Exploring the magnetohydrodynamic stretched flow of Williamson Maxwell nanofluid through porous matrix over a permeated sheet with bioconvection and activation energy, Sci. Rep. 12 (1) (2022) 1–12.
[42] A. Ali, S. Sarkar, S. Das, R.N. Jana, A report on entropy generation and Arrhenius kinetics in magneto-bioconvective flow of Cross nanofluid over a cylinder with wall slip, Int. J. Ambient Energy (2022) 1–16.
[43] Z. Ullah, I. Ullah, G. Zaman, T.C. Sun, A Numerical Approach to Interpret Melting and Activation Energy Phenomenon on the Magnetized Transient Flow of Prandtl–Eyring Fluid with the Application of Cattaneo–Christov Theory, Waves in Random and Complex Media, 2022, pp. 1–21.
[44] I. Ullah, Activation energy with exothermic/endothermic reaction and Coriolis force effects on magnetized nanomaterials flow through Darcy–Forchheimer porous space with variable features, Waves Random Complex Media (2022) 1–14.
[45] F.S. Al-Mubaddel, F.M. Allehiany, T.A. Nofal, M.M. Alam, A. Ali, J.K.K. Asamoah, Rheological model for generalized energy and mass transfer through hybrid nanofluid flow comprised of magnetized cobalt ferrite nanoparticles, J. Nanomater. 2022 (2022) 1–11.
[46] V. Puneeth, R. Anandika, S. Manjunatha, M.I. Khan, M.I. Khan, A. Althobaiti, A.M. Galal, Implementation of modified Buongiorno's model for the investigation of chemically reacting rGO-Fe3O4-TiO2-H2O ternary nanofluid jet flow in the presence of bio-active mixers, Chem. Phys. Lett. 786 (2022), 139194.
[47] E.A. Algehyne, M. Arif, A. Saeed, M. Bilal, P. Kumam, A.M. Galal, Modified Buongiorno's model for the analysis of chemically reacting jet flow of ternary hybrid nanofluid under the influence of activation energy and bio-active mixers, ZAMM-Journal of Applied Mathematics and Mechanics/Zeitschrift für Angewandte Mathematik und Mechanik (2023), e202200498.
[48] K.A.M. Alharbi, A.E.S. Ahmed, M. Ould Sidi, N.A. Ahammad, A. Mohamed, M.A. El-Shorbagy, R. Marzouki, Computational valuation of Darcy ternary-hybrid nanofluid flow across an extending cylinder with induction effects, Micromachines 13 (4) (2022) 588.
[49] A. Ahmadian, M. Bilal, M.A. Khan, M.I. Asjad, Numerical analysis of thermal conductive hybrid nanofluid flow over the surface of a wavy spinning disk, Sci. Rep. 10 (1) (2020) 1–13.
[50] W.A. Khan, I. Pop, Boundary-layer flow of a nanofluid past a stretching sheet, Int. J. Heat Mass Tran. 53 (11–12) (2010) 2477–2483.
[51] C.Y. Wang, Free convection on a vertical stretching surface, ZAMM-Journal of Applied Mathematics and Mechanics/Zeitschrift für Angewandte Mathematik und Mechanik 69 (11) (1989) 418–420.